Perturbation analysis of entrainment in a micromechanical limit cycle oscillator

Manoj Pandey *, Richard Rand, Alan Zehnder

Department of Theoretical and Applied Mechanics, Cornell University, Kimball Hall, Ithaca, NY 14853-1503, United States

Abstract

We study the dynamics of a thermo-mechanical model for a forced disc shaped, micromechanical limit cycle oscillator. The forcing can be accomplished either parametrically, by modulating the laser beam incident on the oscillator, or non-parametrically, using inertial driving. The system exhibits both 2:1 and 1:1 resonances, as well as quasiperiodic motions and hysteresis. A perturbation method is used to derive slow flow equations, which are then studied using the software packages AUTO and pplane7. Results show that the model agrees well with experiments. Details of the slow flow behavior explain how and where transitions into and out of entrainment occur.
© 2006 Elsevier B.V. All rights reserved.

1. Introduction

Entrainment is the phenomenon in which freely oscillating systems, synchronize with each other or with an external force. Entrainment can occur in numerous physical, chemical, biological and sociological systems. Examples of such systems include entrainment of human circadian rhythms by light, where the biological clock is entrained to the cycle of day and night [1], radio frequency systems [2], superconducting Josephson junction arrays [3] and the mutual entrainment of fireflies [4] which glow in unison after synchronization.

In this paper, we use perturbation methods to analyze the entrainment behavior exhibited by a planar, disc-shaped micromechanical limit cycle oscillator. The oscillator, shown in Fig. 1, consists of a thin circular plate of single crystal Si supported above a Si substrate by a SiO$_2$ pillar [5,6]. A constant (CW) laser beam, focused to a 5 μm spot near the edge of the disc, is used both to detect the vibrations and to drive the disc. The disc is thin enough that much of the incident laser light is transmitted through the disc and then reflected back by the Si substrate below. This process repeats itself in a series of reflections and transmissions, the net result of which

---

* Corresponding author. Tel.: +1 607 255 0824; fax: +1 607 255 2011.
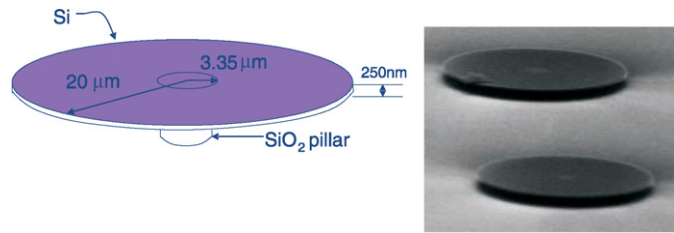 *E-mail address:* mp252@cornell.edu (M. Pandey).

Fig. 1. Disk-shaped oscillator. Right: SEM image of actual structure. From [5].

is that the disc-substrate system forms a Fabry–Perot interferometer. Both the net reflected and the net absorbed light vary periodically with the deflection of the disc at the point of illumination. Thus the laser can be used to interferometrically detect vibrations of the disc. In addition, the amount of heat absorbed and hence the thermal strains also vary with disc deflection. The oscillatory thermal strains produce a thermal drive of the disc and they modulate the disc's stiffness [7]. Since the thermal driving force depends on the position of the disc, the system has feedback that can cause the rest position of the disc to become unstable when the laser power exceeds a threshold, driving the disc into limit cycle motions via a Hopf bifurcation [7].

In the experiments [5] the CW laser power was increased to a level just beyond the threshold for limit cycle oscillations. Once the disc was oscillating, it was found that the frequency of vibration can be tuned by applying a ''pilot signal'' consisting of either a modulation of the incident laser beam or an inertial drive provided by a modulated piezoelectric actuator taped to the back of the chip containing the disc. If the frequency of modulation of the pilot is close to the limit cycle frequency of the oscillator, the oscillator locks itself onto the pilot signal and remains locked in frequency and phase over a range of frequencies. The disc is said to have been entrained by the pilot signal. If the pilot frequency is not close to the oscillator limit cycle frequency, then the oscillator continues to oscillate at its own frequency and phase. The system exhibits hysteresis, that is, the entrainment region obtained when sweeping backward in frequency has different boundaries than the comparable region obtained when sweeping forward. The amplitude and the frequency response for the case of inertial (piezo) pilot signal are shown in Figs. 2 and 3. See [5] for further details of the experiments.

Modeling of this device and numerical simulations of the governing equations have been discussed earlier in [7–9]. Here we use perturbation theory to discern additional details of the transitions into and out of entrainment that are not amenable to numerical simulations. The model equations for this system are [7,9]:

$$\ddot{z} + \frac{1}{Q}(\dot{z} - D\dot{T}) + (1 + CT)(z - DT + \beta(z - DT)^3) = M \sin(\omega_{\text{piezo}} t), \tag{1}$$

$$\dot{T} + BT = AP, \tag{2}$$

and

$$P = P_{\text{laser}}(1 + \varphi \cos(\omega_{\text{laser}} t))(\alpha + \gamma \sin^2(2\pi(z - z_0))). \tag{3}$$
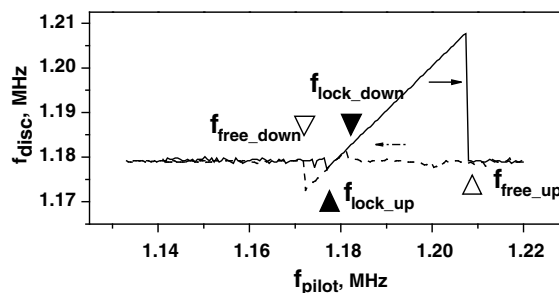

Fig. 2. Frequency of response versus piezo forcing frequency, obtained experimentally. From [5].
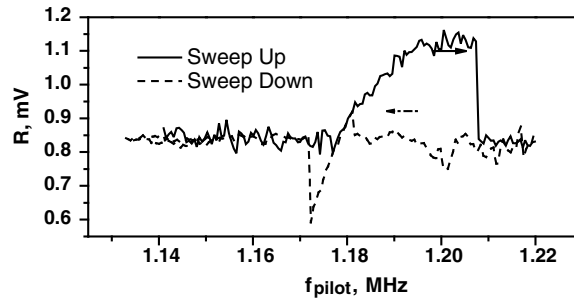
Fig. 3. Amplitude of response versus piezo forcing frequency, obtained experimentally. Amplitude shown as mV output from photodetector. Actual amplitude of motion is shown in [7] to range from 80–160 nm, or 0.13–0.26 λ, where λ is the wavelength of the incident light. From [5].

where z represents the displacement of the disc at the location of the focused laser beam and z_0 represents its equilibrium position. Both these quantities have been normalized by the wavelength of the incident light. T is the temperature of the disc. M represents the amplitude of the inertial (piezo) drive. P_{laser} is the CW laser power while φ is the amplitude of the AC laser signal. C is the relative change in spring constant per unit temperature change. D is the deflection of the disk due to heating, per unit temperature change. B represents the disk's overall thermal conductivity and A its overall thermal mass. β is the non-linearity in the disk's stiffness. Time in Eqs. (1)–(3) has been scaled by the natural frequency of the undamped linear oscillator and hence the natural frequency is 1. For a disc oscillator of outer diameter 35 μm and the inner diameter 7 μm that has a natural frequency of 1.2 MHz for the $(0,0)$ mode, oscillating in vacuum, the parameters in the above equations are estimated to be [7]

$$Q = 10\,000, \quad \beta = 0.4, \quad A = 0.0176\,^\circ\text{C}/\mu\text{W}, \quad B = 0.488, \quad C = 3.53 \times 10^{-4}/^\circ\text{C},$$
$$D = 1.3 \times 10^{-5}/^\circ\text{C}, \quad M = 0.000025, \quad \alpha = 0.06, \quad \gamma = 0.26, \quad z_0 = 0.064 \tag{4}$$

It is to be noted that although Eqs. (1)–(3) involve two independent forcing frequencies, namely ω_{piezo} and ω_{laser}, we consider only scenarios in which these are applied one at a time. The reason is that entrainment is not expected to occur unless the system is driven by a single forcing frequency.

We first summarize the motion predicted by the above system of equation. If the disc is heated with a continuous wave (CW) laser beam of power above the Hopf bifurcation threshold, a stable limit cycle of finite amplitude exists in the system [7]. If a modulated signal is also applied to the oscillator either in the form of inertial piezo drive or via a modulated laser beam, the system becomes a non-autonomous one and the limit cycle becomes either a quasiperiodic motion, if the limit cycle and pilot signal frequencies are not close, or becomes a periodic motion at the pilot signal frequency if the frequencies are sufficiently close. If the laser power were to be switched-off, so that the only forcing is coming from the piezo drive, then the system reduces to a forced Duffing oscillator and hence shows a backbone-shaped amplitude–frequency response [10].

2. Numerical results

The numerical results for the above equations are discussed extensively in [9]. Fig. 4 shows the response amplitude versus piezo forcing frequency for a case when P_{laser} is above the Hopf bifurcation threshold and hence the limit cycle exists. We look at the case of 1:1 entrainment of the disc by the piezo drive. For a frequency of 0.98 all the initial conditions lead to a limit cycle motion of amplitude around 0.25. The frequency response of the system is at the limit cycle frequency as seen from Fig. 5. As the forcing frequency is increased the limit cycle persists until a frequency of 1.008 at which the system jumps onto a lower amplitude motion, which occurs at a specific piezo forcing frequency. The disc is said to have been entrained by the forcing. It remains entrained until the forcing frequency reaches 1.045, during which its amplitude as well as its frequency increase steadily. After entrainment is lost the motion jumps back to the limit cycle. If the forcing frequency is swept backwards, the system stays on the limit cycle until a frequency of 1.012 where it is again
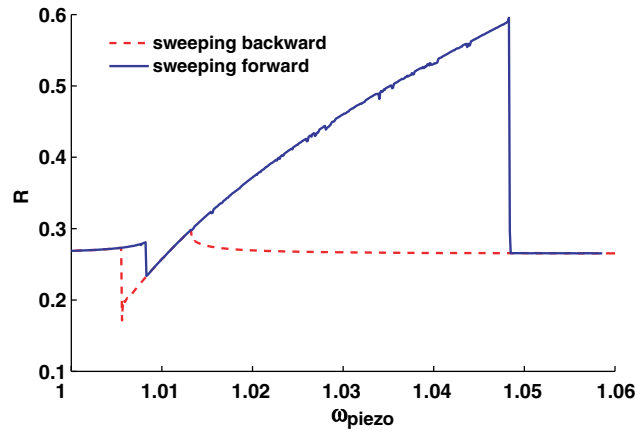
Fig. 4. Amplitude of response versus frequency of piezo drive, obtained by numerical integration of Eqs. (1)–(3). $M = 0.0001$, $\varphi = 0.0$, $P_{laser} = 650\,\mu W$ for 1:1 piezo-modulation. From [9].
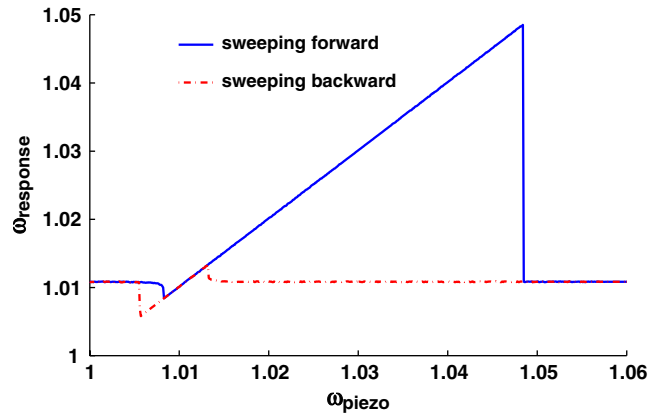

Fig. 5. Frequency of response versus frequency of piezo drive, obtained by numerical integration of Eqs. (1)–(3). $M = 0.0001$, $\varphi = 0.0$, $P_{laser} = 650\,\mu W$ for 1:1 piezo-modulation. From [9].

entrained and remains so until a frequency of 1.005 when the system jumps back to the limit cycle. Since the region of entrainment while sweeping forward is different from the one sweeping back, we see hysteresis in the system. Similar behavior is seen when the laser beam is modulated, with no piezo drive.

3. Perturbation results

We apply the two variable expansion perturbation method [10] to the governing Eqs. (1) and (3). This involves replacing time t by two time scales, stretched time $\xi = \omega t$ and slow time $\eta = \epsilon t$. Here ω is taken as the forcing frequency, that is, either $\omega = \omega_{piezo}$ or $\omega = \omega_{laser}$, depending upon which type of forcing we are considering. (Recall we do not consider examples in which both types of forcing are applied.) To make the following analysis concrete, we will omit laser modulation by taking $\varphi = 0$ in Eq. (3), and we will choose $\xi = \omega_{piezo}t$.

Next, the displacement z and temperature T are expanded in a series of ϵ:

$$z = Z_0(\xi, \eta) + \epsilon Z_1(\xi, \eta) + \mathrm{O}(\epsilon^2) \tag{5}$$
$$T = T_0(\xi, \eta) + \epsilon T_1(\xi, \eta) + \mathrm{O}(\epsilon^2) \tag{6}$$

The forcing frequency $\omega = \omega_{\text{piezo}}$ is detuned-off of the natural frequency of the oscillator, which has been scaled to 1 in Eq. (1):

$$\omega = 1 + \epsilon k_1 + \mathrm{O}(\epsilon^2) \tag{7}$$

The equation parameters are scaled so that when $\epsilon = 0$ Eq. (1) becomes a simple harmonic oscillator:

$$Q = \frac{Q'}{\epsilon}, \quad C = C'\epsilon, \quad D = D'\epsilon, \quad \beta = \beta'\epsilon, \quad M = M'\epsilon \tag{8}$$

In what follows we make these substitutions in Eqs. (1) and (3), and then drop the primes for convenience.

Making the substitutions (5)–(8) in Eqs. (1) and (2) and collecting terms in ϵ gives a sequence of differential equations on Z_i and T_i, the first few of which are:

$$\frac{\partial^2 Z_0}{\partial \xi^2} + Z_0 \tag{9}$$

$$\frac{\partial T_0}{\partial \xi} - B T_0 = AP \tag{10}$$

$$\frac{\partial^2 Z_1}{\partial \xi^2} + Z_1 = M \sin \xi - 2k_1 \frac{\partial^2 Z_0}{\partial \xi^2} - 2 \frac{\partial^2 Z_0}{\partial \xi \partial \eta} - \frac{1}{Q} \frac{\partial Z_0}{\partial \xi} - C T_0 Z_0 + D T_0 - \beta Z_0^3 \tag{11}$$

The general solution of Eq. (9) is of the form

$$Z_0(\xi, \eta) = X(\eta) \cos \xi + Y(\eta) \sin \xi \tag{12}$$

where $X(\eta)$ and $Y(\eta)$ are slowly varying coefficients.

In order to obtain a closed form solution to Eq. (10), the $\sin^2 2\pi(Z_0 - z_0)$ term in P (see Eq. (3)) is approximated by the following truncated Taylor expansion, valid for small values of $(Z_0 - z_0)$:

$$\sin^2 2\pi(Z_0 - z_0) \approx 4\pi^2(Z_0 - z_0)^2 + \frac{16\pi^4}{3}(Z_0 - z_0)^4 \tag{13}$$

After substituting Eqs. (12),(13) and (3) into Eq. (10), we used the computer algebra software MACSYMA to solve for the steady state solution T_0. This gives a very large expression which we omit here for brevity. The expression for T_0 so obtained is then substituted, along with Eq. (12), into Eq. (11). Then after trigonometric simplification, we proceed with the removal of the secular terms, these being the coefficients of $\sin \xi$ and $\cos \xi$. The result is a pair of slow flow equations which govern the evolution of the slowly varying coefficients $X(\eta)$ and $Y(\eta)$. Since these equations are very long if written out with all the parameters in unevaluated form, we present instead a version of the slow flow which uses the numerical values of the coefficients listed in Eq. (4) and $P_{\text{laser}} = 650 \ \mu W$:

$$\begin{aligned} \dot{X} = &-M + a_{1,0}X + a_{0,1}Y + a_{3,0}X^3 + a_{2,1}YX^2 + a_{1,2}Y^2X + a_{0,3}Y^3 + a_{5,0}X^5 + a_{4,1}YX^4 \\ &+ a_{3,2}Y^2X^3 + a_{2,3}Y^3X^2 + a_{1,4}Y^4X + a_{0,5}Y^5 \end{aligned} \tag{14}$$

$$\begin{aligned} \dot{Y} = &\ b_{1,0}X + b_{0,1}Y + b_{3,0}X^3 + b_{2,1}YX^2 + b_{1,2}Y^2X + b_{0,3}Y^3 + b_{5,0}X^5 + b_{4,1}YX^4 \\ &+ b_{3,2}Y^2X^3 + b_{2,3}Y^3X^2 + b_{1,4}Y^4X + b_{0,5}Y^5 \end{aligned} \tag{15}$$

where the numerical value of the coefficients $a_{i,j}$ and $b_{i,j}$ is given in the Appendix.

The slow flow equations can be used for an extended analysis of the original system of equations at a much smaller computer budget. Fixed points of the slow flow (14), (15) correspond to periodic motions (limit cycles) in the original system, Eqs. (1)–(3) [11]. Similarly, limit cycles of the slow flow correspond to quasiperiodic motions in the original system [11].

Our numerical procedure can be summarized as follows. One of the fixed points of the slow flow (14), (15) is solved for numerically. Then using the continuation software AUTO, the locus of these fixed points is found as the detuning parameter k_1 is varied. Similarly the locus of all slow flow limit cycles can be obtained as a function of detuning. The resulting plot is shown in Fig. 6. Phase plane plots are shown in Fig. 7 for various regions in Fig. 6. The following discussion is aimed at explaining the features of these figures.
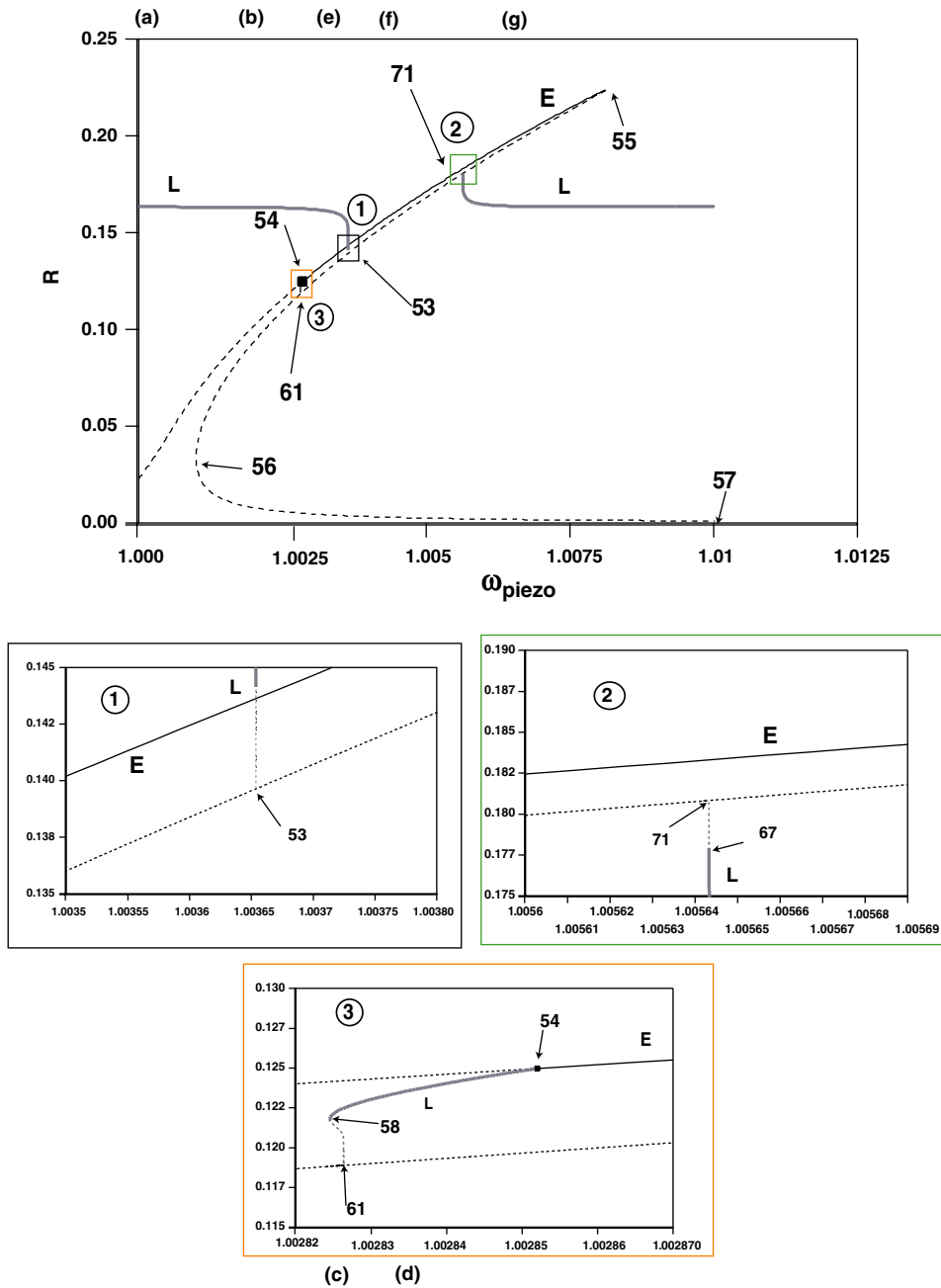
Fig. 6. 1:1 Entrainment using piezo drive based on perturbation slow flow Eqs. (14), (15). $P_{\text{laser}} = 650\ \mu\text{W}$, $\varphi = 0$. 'L' denotes limit cycle in the slow flow, which corresponds to quasiperiodic motion in the original system (1)–(3), while 'E' is the entrained region which corresponds to stable fixed points in the slow flow. A solid line represents stable motion while a dashed line represents unstable motion. The insets contain close up views. Insets (1) and (2) show the disappearance of the limit cycle in a homoclinic bifurcation. Inset (3) shows how entrainment is lost while sweeping backward in frequency due to a supercritical Hopf bifurcation, see text. The letters (a), (b), ... mark the frequencies for which the phase portraits are shown in Fig. 7.

Away from the resonance all initial conditions lead to motions which approach the limit cycle (labeled L). There exists an unstable slow flow fixed point close to the origin as well. The corresponding slow flow phase portrait is subfigure (a) of Fig. 7. As the forcing frequency is increased, the slow flow fixed point follows a backbone curve which corresponds to the associated Duffing oscillator (that is, to Eq. (1) with $C = D = 0$).
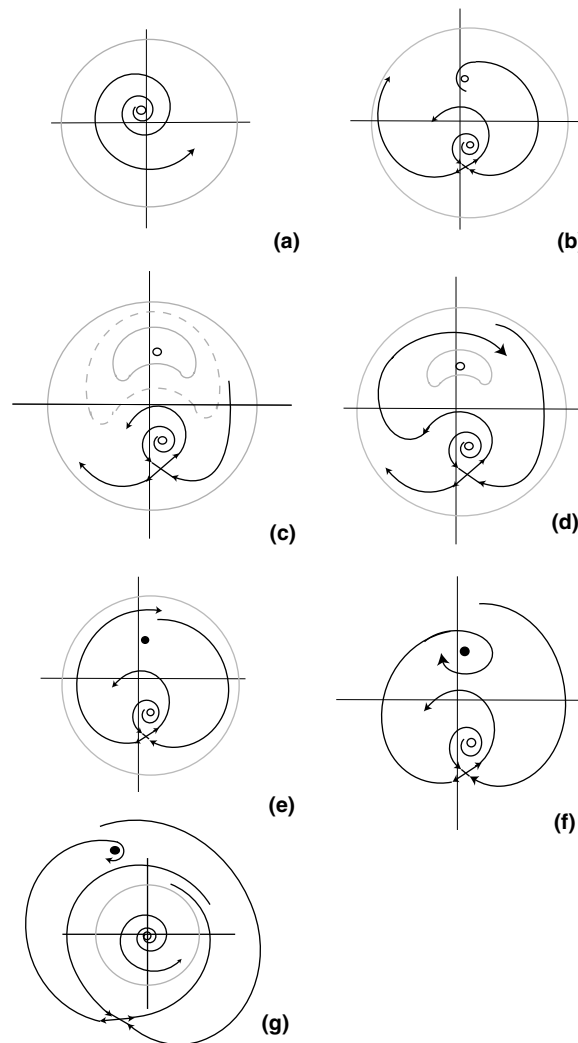
Fig. 7. Phase portraits corresponding to Fig. 6 at different frequencies. (a) to the left of point 56 and to the right of point 55; (b) between points 56 and 58; (c) between points 58 and 61; (d) between points 61 and 54; (e) between points 54 and 53; (f) between points 53 and 71 and (g) between points 71 and 55. Empty circles represent the unstable fixed points, filled circles the stable fixed points and closed orbits in lighter color the limit cycles in slow flow.

A saddle-node bifurcation occurs at the point labeled 56, and the phase portrait now looks like subfigure (b). The stability of the fixed point following the resonance curve changes at the point labeled 54 where it becomes stable. The limit cycle (labeled L) meanwhile is stable and hence motion starting near it would continue to approach it during the forward sweep of the frequency. The phase portrait here is shown in subfigure (e). As the limit cycle approaches the resonance curve, its amplitude starts to decrease and close to point 53 its amplitude–frequency curve becomes vertical and loses stability. At this frequency only the slow flow fixed point is stable and the motion jumps to that. From the phase portrait plots we see that a homoclinic bifurcation takes place in the slow flow, wherein the limit cycle hits the saddle point and disappears, i.e., going from (e) to (f) in Fig. 7. This corresponds in the original system to a transition from quasiperiodic motion (a slow flow limit cycle) to a response at the forcing frequency (a slow flow equilibrium) and the system is said to have been entrained by the forcing. Increasing the forcing frequency beyond this point causes the system to continue on the locus of the stable fixed points of the system,which traces the backbone curve. At 71 a stable limit cycle is born from a homoclinic bifurcation and hence at $\omega = 1.0075$ the phase portrait looks like subplot (g). The motion however remains on the stable fixed point until point 55 where the stable fixed point and the

saddle point disappear in a saddle-node bifurcation. The motion now jumps back to the stable slow flow limit cycle and the phase portrait again looks like (a).

If the frequency is swept in the opposite direction, i.e., from high to low, the system at first stays on the stable slow flow limit cycle. This continues until point 71, where the limit cycle becomes unstable and the motion jumps to the nearby stable slow flow fixed point and the system is entrained. It should be noted that this point is lower in frequency than the point at which entrainment was lost in the forward sweep. This produces hysteresis in the system. The system traces the backbone curve until point 54 where the fixed point becomes unstable, undergoing a supercritical Hopf bifurcation in the slow flow. The corresponding phase portrait is shown in (d). A stable slow flow limit cycle which was born in the Hopf bifurcation now surrounds the unstable fixed point. Another unstable limit cycle is born at 61 in a homoclinic bifurcation and the phase plane plot (c) shows that it surrounds the stable limit cycle. These two slow flow limit cycles disappear in a cyclic fold bifurcation at point 58 shown in inset 3. The system now jumps back to the limit cycle L and entrainment is lost as the forcing frequency is decreased. The phase plane now looks like (b). Decreasing frequency further causes the phase plane to again look like (a) after a saddle-node bifurcation at point 56.

We note that Eqs. (14), (15) and Figs. 6 and 7 apply to the system (1)–(3) which is driven by piezo forcing. We now consider the case in which the piezo drive is switched-off and the system is driven by modulating the
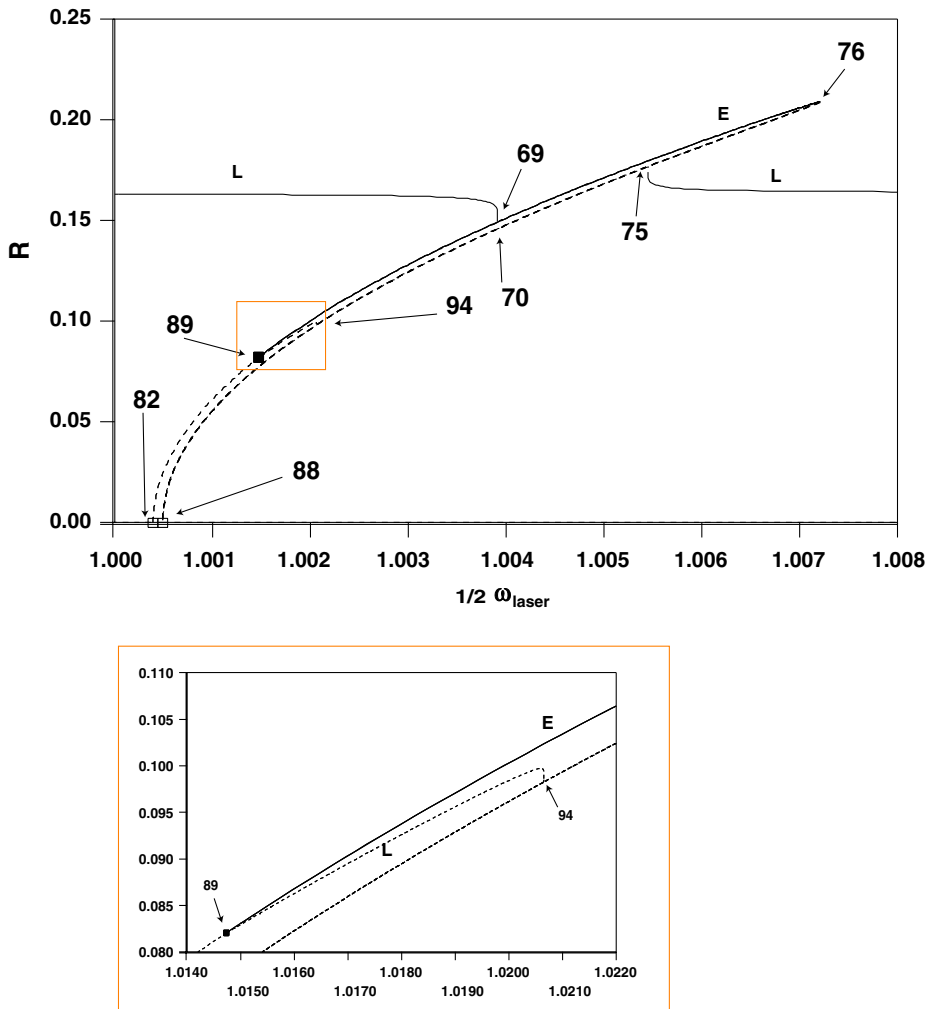

Fig. 8. Entrainment using laser modulation from a perturbation slow flow analysis. $P_{laser} = 650\ \mu W$ and $M = 0$. The inset contains a close-up near the frequency at which entrainment is lost sweeping backwards due to a subcritical Hopf bifurcation.

laser beam at close to twice the natural frequency of the unforced oscillator. We expect 2:1 resonance because of the parametric excitation involved in the term $(1 + CT)(z - DT + \beta(z - DT)^3)$ of Eq. (1). Here T is periodic as shown in the foregoing discussion of the perturbation method, and provides the parametric excitation due to the $(1 + CT)$ coefficient.

Fig. 8 shows the results of a similar perturbation analysis for the case of 2:1 laser modulation forcing. The dynamics in this case are similar to the piezo driven case except that a subcritical Hopf bifurcation takes place at the point where the entrainment is lost as opposed to the supercritical Hopf bifurcation seen in the piezo forcing case.

Next the effect of switching-off some of the terms in the governing equations is studied. Fig. 9 shows the effect of turning-off the C term, i.e., the parametric amplification term in Eq. (1). The slow flow limit cycle
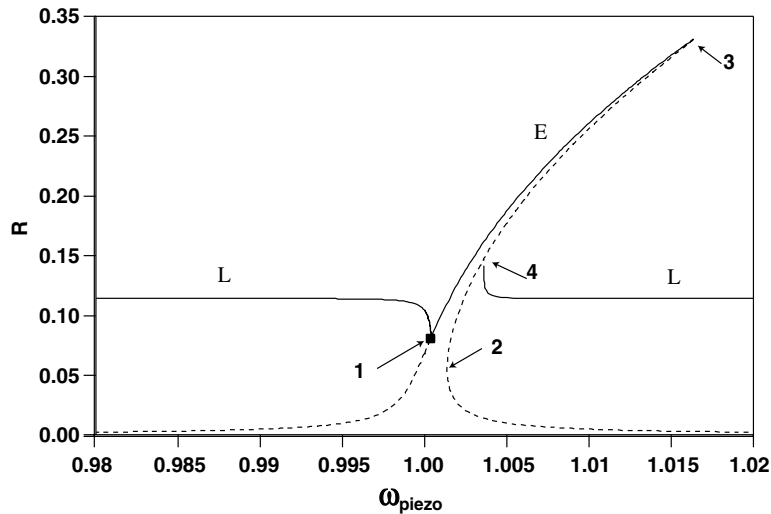

Fig. 9. Entrainment region for piezo forcing with $C = 0$, from a perturbation slow flow analysis. $P_{laser} = 650\,\mu W$ and $\varphi = 0$. 'L' denotes the limit cycle in the slow flow while 'E' is the entrained region which corresponds to a stable fixed point of the slow flow. These results contradict the observed experimental results, showing that the C term is needed to correctly model the physical system.

Fig. 10. Entrainment region for piezo forcing with $D = 0$, from a perturbation slow flow analysis. $P_{laser} = 1650\,\mu W$ and $\varphi = 0$. Solid lines represent stable motion while dashed lines represent unstable motion. 'L' denotes a limit cycle in the slow flow while 'E' is the entrained region which corresponds to a stable fixed point of the slow flow. These results contradict the observed experimental results, showing that the D term is needed to correctly model the physical system.
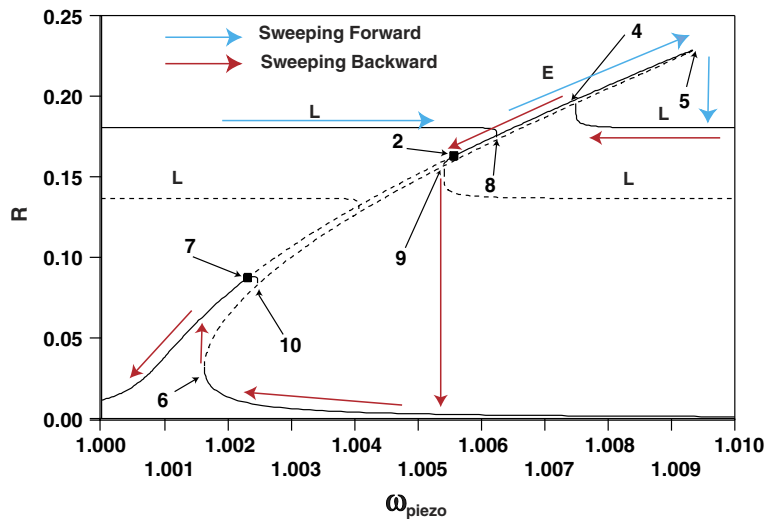
exists but with a smaller amplitude. It is seen that the slow flow limit cycle is born and continues from the point where the fixed point changes its stability, undergoing a Hopf bifurcation (labeled 1 in Fig. 9). Hence the point where the entrainment is lost while sweeping backwards in frequency is the same as the point at which the system gets entrained while sweeping forward. This behavior contradicts that of the physical system as shown in Figs. 2 and 3. Similar behavior, namely that there is no hysteresis and the amplitude is lower when $C = 0$, was seen in the numerical integration of original equations in [9]. Hence the C term is needed to correctly model the physical system.

Removing the effect of heating on the deflection of the disk, i.e., setting $D = 0$, results in the slow flow simulation shown in Fig. 10 for a laser power of 1650 μW. At the laser power of 650 μW (not shown) the system exhibits only the resonant behavior of a Duffing oscillator [10], as the slow flow limit cycle does not exist in the system at this power. It was shown in [7,8] that taking $D \rightarrow 0$ pushes the Hopf bifurcation threshold to a very high value. Hence the limit cycles exist only for very high laser powers and there exists an unstable limit cycle of smaller amplitude along with the stable one. The amplitude frequency curve in Fig. 10 is explained next. While sweeping forward in frequency, the motion would exist on the stable slow flow limit cycle and would become entrained at the point marked eight. It would remain entrained until the point five, after which it jumps down onto a slow flow limit cycle again. While sweeping backwards, the limit cycle would entrain at point four. It remains entrained until point two where the fixed point becomes unstable and a stable limit cycle is born from a Hopf bifurcation. This limit cycle disappears just like in the case of Fig. 6, due to a cyclic fold bifurcation. The motion then jumps down to the resonance curve at point 9. Further decreases in forcing frequency produce a jump up onto the resonance curve at point six. Here there are two stable slow flow states, a stable equilibrium and a stable limit cycle. Their basins of attraction are separated by an unstable limit cycle. After this, the system follows the resonance curve and the amplitude dies out as frequency decreases. Similar behavior was seen in the numerical simulations [9]. The perturbation theory results and the numerical results predict behavior that contradict the observed experimental results, showing that the D term is needed to correctly model the physical system.

4. Conclusion

The results show that analysis of the slow flow equations not only captures the behaviors shown by numerical simulation of the original model Eqs. (1)–(3), but also that they provide an insightful look at the details of the onset and loss of entrainment, explaining the hysteretic jump up and jump down behavior seen experimentally. These results provide a complete picture of the dynamics, including unstable motions and bifurcations which could not be observed from direct numerical integration of original equations. Note that the entrainment limits and amplitudes of periodic motions obtained from the perturbation analysis do not agree exactly with the comparable quantities obtained from the numerical integration of original equations of motion. One source of this disagreement is the approximation (13) used for the $\sin^2 2\pi(Z_0 - z_0)$ term.

Acknowledgements

Appendix

The values of the coefficients in Eqs. (14) and (15) are given below:

$$a_{1,0} = -0.0004296$$
$$a_{0,1} = -0.00044719 - k_1$$
$$a_{3,0} = 0.0000967963$$
$$a_{2,1} = 1.51401$$
$$a_{1,2} = 0.0000967963$$
$$a_{0,3} = 1.51401$$

$$a_{5,0} = -0.21743$$
$$a_{4,1} = -0.21743$$
$$a_{3,2} = -0.06435$$
$$a_{2,3} = -0.43487$$
$$a_{1,4} = -0.03218$$
$$a_{0,5} = -0.21743$$
$$b_{1,0} = -0.00044719 + k_1$$
$$b_{0,1} = -0.00004296$$
$$b_{3,0} = -1.51401$$
$$b_{2,1} = 0.0000967963$$
$$b_{1,2} = -1.51401$$
$$b_{0,3} = 0.0000967963$$
$$b_{5,0} = 0.21743$$
$$b_{4,1} = -0.03218$$
$$b_{3,2} = 0.43487$$
$$b_{2,3} = -0.06435$$
$$b_{1,4} = 0.21743$$
$$b_{0,5} = -0.03218$$

References

[1] Duffy JF, Wright Jr KP. Entrainment of the human circadian system by light. J Biol Rhythm 2005;20(4):326–38.
[2] Pecora LM, Carroll TL. Synchronization in chaotic systems. Phys Rev Lett 1990;64:821824.
[3] Tsang KY, Mirillo RE, Strogatz SH, Weisenfeld K. Dynamics of globally coupled oscillator array. Physica D 1991;48:102.
[4] Mirollo RE, Strogatz SH. Synchronisation of pulse coupled biological oscillators. SIAM J Appl Math 1990;50:1645.
[5] Zalalutdinov M, Aubin K, Pandey M, Zehnder A, Rand R, Houston B, et al. Frequency entrainment for micromechanical oscillator. Appl Phys Lett 2003;83:3281–3.
[6] Zalalutdinov M, Zehnder AT, Olkhovets A, Turner S, Sekaric L, Ilic B, et al. Autoparametric optical drive for micromechanical oscillators. Appl Phys Lett 2001;79:695–7.
[7] Aubin K, Zalalutdinov M, Alan T, Reichenbach R, Rand R, Zehnder A, et al. Limit cycle oscillations in cw laser driven nems. IEEE/ASME J Micromech Syst 2004;13:1018–26.
[8] Zalalutdinov M, Parpia J, Aubin K, Craighead H, Alan T, Zehnder A, et al. Hopf bifurcation in a disk-shaped nems. In: Proc of the 2003 ASME design engineering technical conf, 19th biennial conference on mechanical vibrations and noise, Chicago, IL, September 2–6, 2003, paper no. DETC2003-48516.
[9] Pandey M, Aubin K, Zalalutdinov M, Zehnder A, Rand R. Analysis of frequency locking in optically driven mems resonators. IEEE J Microelectromech Syst, in press.
[10] Rand R. Lecture Notes on Nonlinear Vibrations, version 48. Available online at http://www.tam.cornell.edu/randdocs/, 2005.
[11] Nayfeh AH, Mook DT. Nonlinear Oscillations. NY: Wiley-Interscience; 1979.